Equation-of-State effects on Gravitational Waves in Core-Collapse Supernovae

Oliver Eggenberger Andersen[1] , **Shuai Zha[1]**,
André da Silva Schneider[1], Aurore Betranhandy[1], Sean M. Couch[2,3,4]
and Evan P. O'Connor[1]

[1]The Oskar Klein Centre, Department of Astronomy,
Stockholm University, AlbaNova, SE-106 91 Stockholm, Sweden

[2]Department of Physics and Astronomy,
Michigan State University, East Lansing, MI 48824, USA

[3]Department of Computational Mathematics, Science, and Engineering,
Michigan State University, East Lansing, MI 48824, USA

[4]Facility for Rare Isotope Beams, Michigan State University, East Lansing, MI 48824, USA

Abstract. The nuclear equation-of-state (EOS) describing newly formed proto-neutron stars (PNSs) in core-collapse supernovae (CCSNe) is yet uncertain, and varying its prescription affects multimessenger signatures in CCSN simulations. Focusing on the gravitational wave (GW) signal, we demonstrate the effect of varying parameter values in the EOS. We conclude that an especially important parameter is the effective mass of nucleons which affect thermal properties and subsequently the PNS compactness, regulating the GW signal in both amplitude and frequency. By radially decomposing the GW emission, we show where in the PNS the GWs originate from.

Keywords. supernovae: general, gravitational waves, equation of state, neutrinos

1. Introduction

Induced by the gravitational collapse of the iron core in a massive star, core-collapse supernovae (CCSNe) are the spectacular birth places of neutron-rich and high-temperature compact objects, called proto-neutron stars (PNSs). They either collapse further to a BH or cool down and continue life as a neutron star. The main cooling channel is via neutrino emission. A small fraction of neutrinos may interact with nucleons behind the stalled shock front, driving instabilities in the post-shock region (Couch & Ott 2015). Oscillatory density perturbations of the PNS (Torres-Forné et al. 2018), called PNS oscillations, have been shown to arise when such non-radial motions of matter impinge onto the PNS (Murphy, Ott, & Burrows 2009), which is modeled to be a prominent but yet undetected source of GWs. In CCSNe, photons are obscured by the surrounding material, but GWs and neutrinos may carry information of the physics involved in the initial seconds after collapse. Schneider et al. 2019 show that uncertainties in the thermal part of the nuclear EOS, levered via the effective mass parameter, result in large variations of the PNS structure when compared to uncertainties in the non-thermal EOS.

In this proceeding we present a selection of results based on Eggenberger Andersen et al. 2021 where we investigate the impact of individual parameters in the nuclear equation-of-state (EOS) on the post-bounce dynamics, with focus on the GW signal.
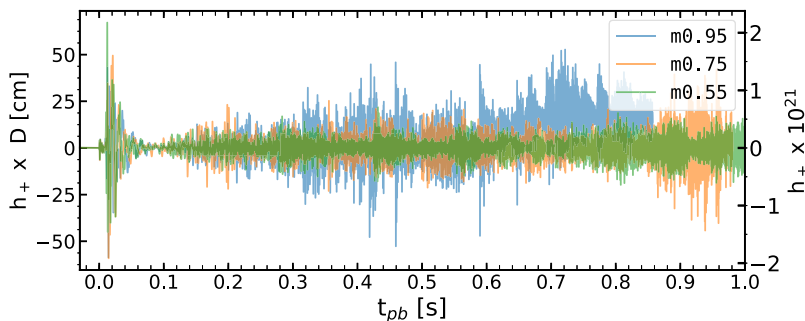
Figure 1. GW signals expressed as the plus polarized strain, h_+, times the equatorial distance to the source, D. The right axis assumes a distance of 10 kpc to the source. The horizontal axis denotes time post-bounce (t_{pb}). Figure from Eggenberger Andersen et al. 2021, © AAS. Reproduced with permission.

2. Equation-of-state

For a detailed account of the EOS prescription, we refer to Schneider et al. 2019 and Eggenberger Andersen et al. 2021. Here we mention that we use a Skyrme-type EOS model (Lattimer & Swesty (1991)) that can be divided into a thermal and a non-thermal part. The non-thermal parameters are fit to reproduce empirical properties of bulk nuclear matter at zero temperature (Schneider et al. 2019). In a meta-modeling approach, these empirical properties are characterized by the coefficients in a Taylor expansion of the specific energy about nuclear saturation density. The thermal part contains the effective mass parameter which does not enter in the expansion, but can be considered a a quasi-empirical parameter (Margueron, Hoffmann Casali, & Gulminelli 2018) and is particularly important for setting the temperature dependence of the nuclear EOS (Schneider et al. 2019). Throughout, the nucleon effective mass is specified as a fraction of the vacuum mass for symmetric nuclear matter at saturation density.

3. Results & Implications

Here we demonstrate the effect of the effective mass, $m^\star$, when varying it with two standard deviations above ($m^\star = 0.95$) and below ($m^\star = 0.55$) the estimated mean ($m^\star = 0.75$) while keeping all other parameters constant. See Eggenberger Andersen et al. 2021 for different rotation rates and results when varying the isoscalar incompressibility parameter in a similar fashion. We have made all GW waveforms publicly available†. The simulations are performed in 2D with imposed axisymmetry utilizing FLASH (Fryxell et al. 2000) and a 20 $M_\odot$ progenitor from Woosley & Heger (2007).

Figure 1 shows the GW amplitude expressed as the plus polarized strain, h_+, times the equatorial distance to the source, D. In general, the GW amplitude increases with the effective mass which we attribute, at least in part, to a general increase in neutrino heating (see bottom panel of Figure 2). This drives stronger instabilities in the post-shock region that act as a forcing mechanism of PNS oscillations (Radice et al. 2019). We do not rule out interior PNS convection as an additional excitation mechanism. Furthermore, a higher neutrino heating makes conditions more favourable for shock revival which is reflected in the top panel of Figure 2 where we see an early shock revival for m0.95, followed by m0.75 towards the end of the simulation time.

The difference in neutrino heating and the subsequent GW amplitude stems from an impact on the thermal pressure throughout the PNS when varying the effective mass (Schneider et al. 2019). This pressure decreases for higher effective mass values, rendering

† GW waveforms available at: https://doi.org/10.5281/zenodo.4973545
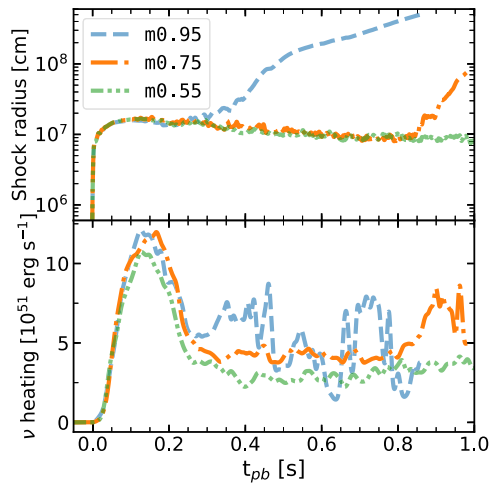
Figure 2. Mean shock radius (*top panel*) and the neutrino heating (*bottom panel*). Shock revival occurs for `m0.95` at ~ 300 ms post-bounce, and for `m0.75` at ~ 900 ms post-bounce. Figure from Eggenberger Andersen et al. 2021, © AAS. Reproduced with permission.
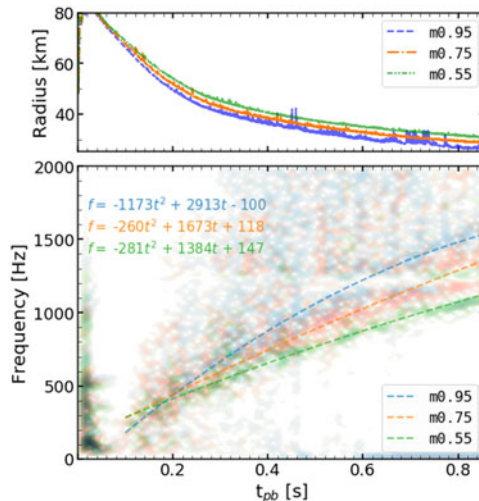
Figure 3. *Top panel*: PNS radius defined as the maximum radius where the density is at least 10^{11} g cm^{-3}. *Bottom panel*: Overlaid spectrograms with second order polynomial fits to the peak frequency. Figure from Eggenberger Andersen et al. 2021, © AAS. Reproduced with permission.

the PNS more compact which releases more binding energy, escaping in the form of neutrinos. The top panel in Figure 3 shows the PNS radius which acts as a proxy for the compactness. A more compact PNS hosts oscillations of higher frequency (Müller, Janka, & Marek 2013), which we demonstrate by overlaying the GW spectrograms in the bottom panel of Figure 3.

Finally, to investigate the spatial origin of the GWs, in Figure 4 we show a radial profile of the `m0.75` spectrogram around two select times, 400 ms (left) and 800 ms (right) post-bounce. To the left of each plot is a projection to easily discern the peak frequency at each epoch which is at roughly 750 Hz at 400 ms and 1200 Hz at 800 ms. In white vertical lines we mark densities $\rho = 10^{11}$, 10^{13}, and 2×10^{14} g cm^{-3}. These roughly divide the PNS core, PNS convection zone, and the convectively-stable PNS surface layer. We conclude
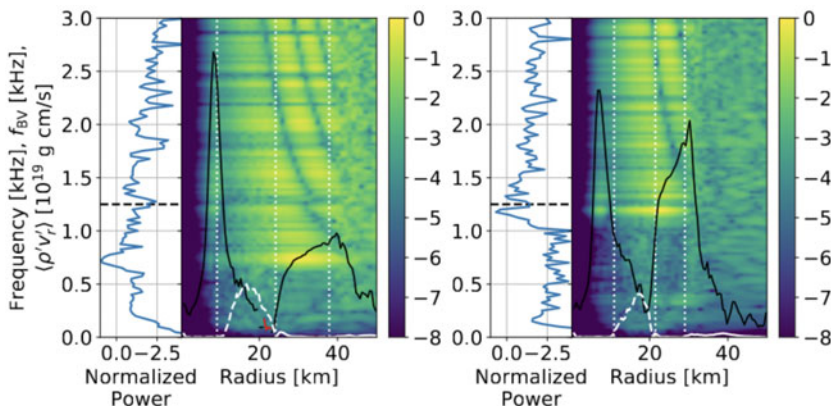
Figure 4. Radial profile of the GW spectrogram for $m^\star = 0.75$ at 400 ms (left) and 800 ms (right). In black we plot the Brunt-Väisälä frequency and in white the turbulent energy flux (negative values in dashed style) to show the convective region. To the left of each plot is a projection of the power spectral density. Figure from Eggenberger Andersen et al. 2021, © AAS. Reproduced with permission.

that the emission is extended throughout the PNS, however, with the surface layer as the dominant emission region, with a tendency towards the bottom end of this layer, this being directly above the convection zone.

The spatial origin of GWs in CCSNe and the excitation mechanism, which both could be highly model dependent, is currently being discussed in the literature (see e.g. Mezzacappa et al. 2020). Groups have shown that interior PNS convection may act as a forcing mechanism on the surface layer from below (Andresen et al. 2017), or that the convection zone itself is the dominant emission region (Mezzacappa et al. 2020). Our results add to the plethora of possibilities and we do not rule out involvement of the convection zone. However, the importance of the interior convection zone compared to the turbulent convection above the PNS require a careful discussion on 2D versus 3D nature (Andresen et al. 2017; Powell & Müller 2019; Eggenberger Andersen et al. 2021). Looking ahead, we encourage a discussion on how spatially dependent the dominant emission region is to the region where the forcing mechanism is doing work.

References

Andresen H., Müller B., Müller E., Janka H.-T., 2017, *MNRAS*, 468, 2032
Couch S. M., Ott C. D., 2015, *ApJ*, 799, 5
Eggenberger Andersen O., Zha S., da Silva Schneider A., Betranhandy A., Couch S. M., O'Connor E. P., 2021, *ApJ*, 923, 201
    doi: 10.3847/1538-4357/ac294c
Fryxell B., Olson K., Ricker P., Timmes F. X., Zingale M., Lamb D. Q., MacNeice P., et al., 2000, *ApJS*, 131, 273
Lattimer J. M., Swesty D. F., 1991, *NuPhA*, 535, 331
Margueron J., Hoffmann Casali R., Gulminelli F., 2018, *PhRvC*, 97, 025805
Mezzacappa A., Marronetti P., Landfield R. E., Lentz E. J., Yakunin K. N., Bruenn S. W., Hix W. R., et al., 2020, *PhRvD*, 102, 023027
Müller B., Janka H.-T., Marek A., 2013, *ApJ*, 766, 43
Murphy J. W., Ott C. D., Burrows A., 2009, *ApJ*, 707, 1173
Radice D., Morozova V., Burrows A., Vartanyan D., Nagakura H., 2019, *ApJL*, 876, L9
Powell J., Müller B., 2019, *MNRAS*, 487, 1178
Schneider A. S., Roberts L. F., Ott C. D., O'Connor E., 2019, *PhRvC*, 100
Torres-Forné A., Cerdá-Durán P., Passamonti A., Font J. A., 2018, *MNRAS*, 474, 5272
Woosley S. E., Heger A., 2007, *PhR*, 442, 269